

Supporting Information

Improving the Optoelectronic Properties of Blue Hybridized Local and Charge-Transfer Emitters via Rational Utilization of Intramolecular Hydrogen Bonds

Xinyong Liu^a, Chenglin Ma^c, Xu Qiu^{*a,b}, Jingwei Li^a, Jiadong Zhou^b,
Shanfeng Xue^{*c}

a. College of Materials Science and Engineering, Shandong University of Science and Technology, Qingdao, 266590, PR China

b. State Key Laboratory of Luminescent Materials and Devices, South China University of Technology, Guangzhou, 510640, PR China

c. School of Polymer Science & Engineering, Qingdao University of Science & Technology, Qingdao, 266042, PR China

* Corresponding authors

E-mail addresses: xqiu@sdust.edu.cn, sfxue@qust.edu.cn

General information

Measurements

^1H and ^{13}C NMR spectra were recorded on a Bruker AC500 (500 MHz) spectrometer at 298 K by utilizing deuterated chloroform (CDCl_3) as the solvent and tetramethylsilane (TMS) as the internal standard. The APCI-MS mass spectra were recorded using a Waters ACQUITY TQD instrument. Elemental analysis was performed on a PerkinElmer 2400. UV-vis absorption spectra were recorded on a Hitachi U-4100 spectrophotometer. Fluorescence measurements were carried out with a Hitachi F-4600 spectrophotometer. The quantum efficiencies of solution and solid films were carried out with FLS980 Spectrometer. Thermal gravimetric analysis (TGA) was undertaken on a PerkinElmer thermal analysis system at a heating rate of $10\text{ }^\circ\text{C min}^{-1}$ and a nitrogen flow rate of 40 mL min^{-1} . Differential scanning calorimetry (DSC) was performed on a NETZSCH (DSC-204) unit at a heating rate of $10\text{ }^\circ\text{C min}^{-1}$ under nitrogen. Cyclic voltammetry (CV) was performed using a BAS 100W (Bioanalytical Systems), using a glass carbon disk (diameter = 3 mm) as the working electrode, a platinum wire with a porous ceramic wick as the auxiliary electrode, and Ag/Ag^+ as the reference electrode standardized by the redox couple ferrocenium/ferrocene. Anhydrous dichloromethane (CH_2Cl_2) containing 0.1 M tetrakis(n-butyl)-ammonium hexafluorophosphate (NBu_4PF_6) as the supporting electrolyte were used as solvents under a nitrogen atmosphere. All solutions were purged with a nitrogen stream for 10 min before measurement. The procedure was performed at room temperature, and a nitrogen atmosphere was maintained over the solution during measurements. A scan rate of 50 mV s^{-1} was applied.

Theoretical calculation

The ground-state geometries were optimized at the BMK/6-31g(d,p) level. On the basis of the optimized configuration of the ground state (S_0), the high excitation energy levels of singlet and triplet states were evaluated also using BMK/6-31g(d,p). In order to gain further insight into the character of excited state, natural transition orbitals (NTOs) were evaluated for $S_1 \rightarrow S_0$ transition. Reduced density gradient (RDG) (*J. Am. Chem. Soc.*,

2010, 132, 6498.) analysis was conducted using the Multiwfn program (version 3.8) (*J. Comput. Chem.*, 2012, 33, 580.), and the corresponding molecular orbitals were visualized using the VMD software.

Device fabrication

Indium–tin oxide (ITO) coated glass with a sheet resistance of 15–20 $\Omega \text{ cm}^{-2}$ was used as the substrate. Before device fabrication, the ITO glass substrates were cleaned with acetone, detergent, deionized water, and isopropanol, dried in an oven at 120 °C, and treated with UV-zone for 20 min. After that, the samples were transferred into a deposition system. The devices were fabricated by the multiple source organic molecular beam deposition method in a vacuum at a pressure of 4×10^{-6} mbar. Evaporation rates of 0.4 \AA s^{-1} for the organic materials and 1–4 \AA s^{-1} for the metal electrodes were applied. The thickness of each deposition layer was monitored using a quartz crystal thickness/ratio monitor (STM-100/MF, Sycon). The EL spectra were measured using a PR650 fluorescence spectrophotometer. The current density–voltage–luminance (J–V–L) characteristics were performed simultaneously by using a computer-controlled source meter (Keithley 2400) equipped with a light intensity meter LS-110 under ambient atmosphere without encapsulation. The EQEs were calculated from the luminance, current density and EL spectrum. All the results of devices were measured in the forward-viewing direction without any out-coupling enhancement techniques.

Synthesis

Starting materials and solvents were purchased from Aldrich Chemical Co., or Energy Chemical Co., China. They were used without further purification. Scheme S1 presents the synthetic routes of mP9PCZ and mPmPCZ.

2-(6-bromopyridin-3-yl)-1-phenyl-1H-phenanthro[9,10-d]imidazole (PI-PBr):

A mixture of aniline (5.0 g, 53.6 mmol), 9,10-phenanthrenequinone (2.2 g, 10.7 mmol), 6-bromo-3-pyridinecarboxaldehyde (2.0 g, 10.7 mmol), ammonium acetate (3.31 g, 42.9 mmol), and acetic acid (30 mL) was refluxed under nitrogen in a 120 °C oil bath for 2 hours. After cooling down, the solid product was filtrated and washed with 30 mL

1:1 water/acetic acid and 30 mL water successively. Then, the solid mixture dissolved in dichloromethane and dried with anhydrous magnesium sulphate, purified by thin layer chromatography using dichloromethane/ethyl acetate (40:1 v/v) as eluent to give the product as white solid and the product yield was (3.05 g, yield: 63.0 %). ¹H NMR (500 MHz, CDCl₃) δ 8.77 (d, J = 8.3 Hz, 1H), 8.70 (d, J = 8.2 Hz, 1H), 8.38 (s, 1H), 7.73 (ddt, J = 31.6, 15.1, 7.4 Hz, 5H), 7.55 (dt, J = 17.1, 7.7 Hz, 4H), 7.29 (t, J = 7.4 Hz, 3H), 7.13 (d, J = 8.1 Hz, 1H).

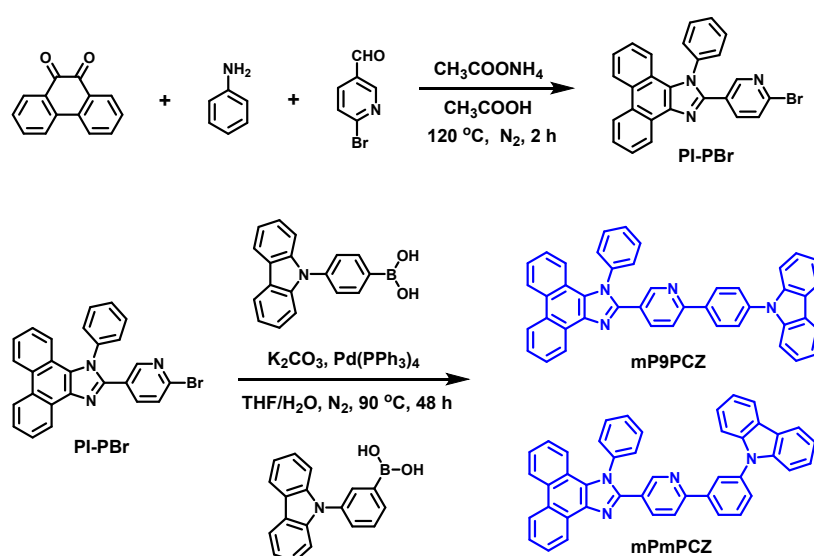
2-(6-(4-(9H-carbazol-9-yl)phenyl)pyridin-3-yl)-1-phenyl-1H-phenanthro[9,10-d]imidazole (mP9PCZ):

A mixture of PI-PBr (1.0 g, 2.2 mmol), 4-(9-carbazolyl)benzeneboronic acid (0.8 g, 2.8 mmol), potassium carbonate (0.5 g, 3.6 mmol), tetrahydrofuran (50 mL) and deionized water (10 mL), with Pd(PPh₃)₄ (0.1 g, 0.09 mmol) acting as a catalyst was refluxed at 90 °C for 48 hours under nitrogen. After the mixture was cooled down, 40 mL deionized water was added to the resulting solution and the mixture was extracted with dichloromethane for three times. The organic phase was dried over anhydrous magnesium sulphate. After filtration and solvent evaporation, the given residue was purified through silica gel column chromatography using dichloromethane/ethyl acetate (40:1 v/v) as eluent to give the product as light yellow solid (1.1 g, yield: 81 %). ¹H NMR (500 MHz, CDCl₃) δ 8.85 – 8.76 (m, 2H), 8.74 (d, J = 8.2 Hz, 1H), 8.26 (d, J = 8.1 Hz, 2H), 8.16 (d, J = 7.7 Hz, 2H), 7.93 (s, 1H), 7.88 – 7.81 (m, 1H), 7.74 (dd, J = 21.0, 7.6 Hz, 6H), 7.63 (dd, J = 21.6, 7.2 Hz, 4H), 7.49 (d, J = 8.2 Hz, 2H), 7.43 (t, J = 7.4 Hz, 2H), 7.32 (q, J = 9.0, 7.3 Hz, 3H), 7.18 (d, J = 8.1 Hz, 2H). ¹³C NMR (126 MHz, CDCl₃) δ 140.59, 139.78, 136.41, 131.22, 131.15, 128.99, 128.97, 128.93, 128.70, 127.25, 127.22, 126.21, 126.15, 126.11, 124.49, 123.67, 123.59, 123.22, 121.13, 120.39, 120.32, 109.84. ESI-MS [M]⁺ *m/z*: 613.2405. Anal. Calcd. (%) for C₄₄H₂₈N₄: C, 86.25; H, 4.61; N, 9.14; Found: C, 86.36; H, 4.72; N, 8.92.

2-(6-(3-(9H-carbazol-9-yl)phenyl)pyridin-3-yl)-1-phenyl-1H-phenanthro[9,10-d]imidazole (mPmPCZ):

A mixture of PI-PBr (1.0 g, 2.2 mmol), 3-(9H-carbazol-9-yl)phenylboronic acid (0.8 g, 2.8 mmol), potassium carbonate (0.5 g, 3.6 mmol), tetrahydrofuran (50 mL) and

deionized water (10 mL), with Pd(PPh₃)₄ (0.1 g, 0.09 mmol) acting as a catalyst was refluxed at 90 °C for 48 hours under nitrogen. After the mixture was cooled down, 40 mL deionized water was added to the resulting solution and the mixture was extracted with dichloromethane for three times. The organic phase was dried over anhydrous magnesium sulphate. After filtration and solvent evaporation, the given residue was purified through silica gel column chromatography using dichloromethane/ethyl acetate (40:1 v/v) as eluent to give the product as white solid (1.2 g, yield: 88 %). ¹H NMR (500 MHz, CDCl₃) δ 8.99 – 8.89 (m, 1H), 8.85 (d, J = 2.0 Hz, 1H), 8.81 – 8.74 (m, 1H), 8.70 (d, J = 8.2 Hz, 1H), 8.19 (d, J = 1.7 Hz, 2H), 8.11 (dd, J = 8.3, 2.2 Hz, 1H), 7.85 (t, J = 1.7 Hz, 1H), 7.84 – 7.78 (m, 1H), 7.78 – 7.74 (m, 1H), 7.72 (d, J = 1.5 Hz, 2H), 7.71 – 7.66 (m, 5H), 7.62 – 7.56 (m, 2H), 7.53 (ddd, J = 8.4, 7.0, 1.3 Hz, 1H), 7.50 – 7.44 (m, 4H), 7.43 – 7.35 (m, 2H), 7.33 – 7.26 (m, 1H), 7.18 (dd, J = 8.4, 1.3 Hz, 1H). ¹³C NMR (126 MHz, CDCl₃) δ 156.82, 149.49, 147.87, 142.44, 140.95, 139.55, 138.34, 137.55, 137.36, 130.57, 130.37, 129.54, 129.01, 128.81, 128.58, 128.45, 127.60, 127.48, 127.38, 127.14, 126.93, 126.42, 125.95, 125.27, 125.18, 124.89, 124.18, 123.17, 122.86, 122.82, 120.92, 120.02. ESI-MS [M]⁺ *m/z*: 613.2394. Anal. Calcd. (%) for C₄₄H₂₈N₄: C, 86.25; H, 4.61; N, 9.14; Found: C, 86.40; H, 4.67; N, 8.93.



Scheme S1. The synthetic procedures of mP9PCZ and mPmPCZ.

Table S1. Crystal data and structural refinement for mP9PCZ and mPmPCZ crystals.

Identification code	mP9PCZ	mPmPCZ
Chemical formula	C ₄₄ H ₂₈ N ₄	C ₄₄ H ₂₈ N ₄
Formula weight	612.70	612.70
Crystal system	monoclinic	triclinic
<i>a</i> /Å	18.8335(4)	9.2039(3)
<i>b</i> / Å	5.62960(10)	9.4040(4)
<i>c</i> / Å	29.0221(5)	18.0371(4)
α /°	90	96.637(3)
β /°	100.602(2)	90.417(2)
γ /°	90	98.521(3)
Unit cell volume/ Å ³	3024.54(10)	1533.12(9)
Temperature/K	149.99(10)	150.00(10)
Space group	P2 ₁ /n	P-1
<i>Z</i>	4	2
Density (calculated) /g cm ⁻³	1.346	1.327
F(000)	1280.0	640.0
2 θ range for data collection/°	5.19 to 148.392	9.576 to 134.132
Index ranges	-21 ≤ <i>h</i> ≤ 23, -3 ≤ <i>k</i> ≤ 6, -35 ≤ <i>l</i> ≤ 34	-8 ≤ <i>h</i> ≤ 10, -11 ≤ <i>k</i> ≤ 11, -21 ≤ <i>l</i> ≤ 21
Reflections collected	17346	13822
Independent reflections	5926	5376
<i>R</i> _{int}	0.0211	0.0231
Data / restraints / parameters	5926 / 0 / 433	5376 / 10 / 446
Goodness-of-fit on <i>F</i> ²	1.027	1.043
Final <i>R</i> _{<i>I</i>} values (<i>I</i> ≥ 2σ(<i>I</i>))	0.0355	0.0489
Final <i>wR</i> (<i>F</i> ²) values (<i>I</i> ≥ 2σ(<i>I</i>))	0.0864	0.1326
Final <i>R</i> _{<i>j</i>} values (all data)	0.0423	0.0545
Final <i>wR</i> (<i>F</i> ²) values (all data)	0.0901	0.1370
CCDC number	2255990	2255989

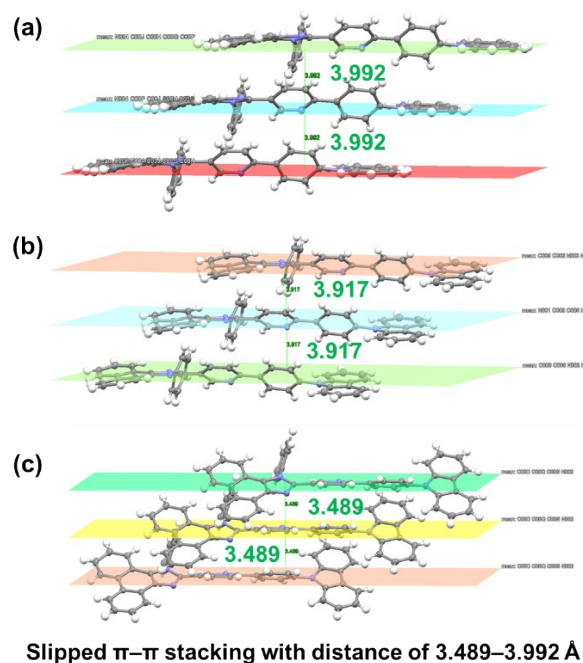


Fig. S1. Slipped π - π stacking with distance of 3.489–3.992 Å in the single-crystal of mP9PCZ.

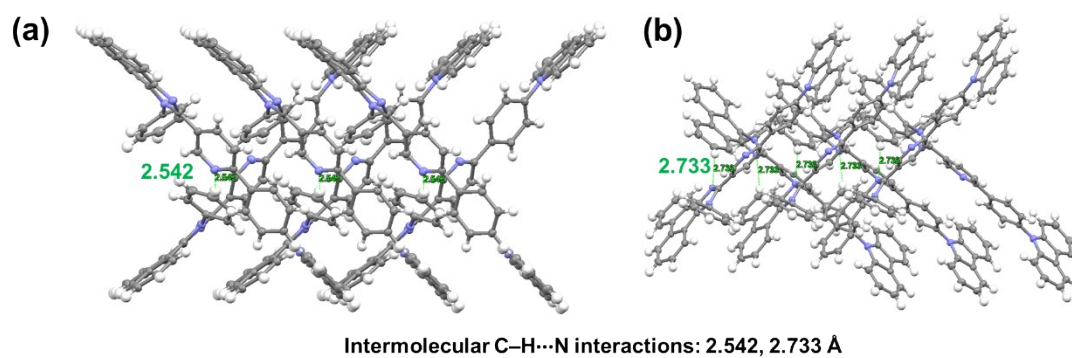


Fig. S2. Intermolecular C-H...N interactions with distance of 2.542, 2.733 Å in the single-crystal of mP9PCZ.

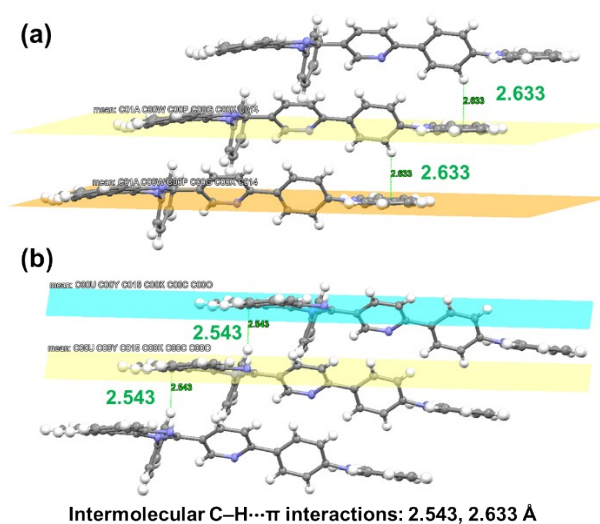


Fig. S3. Intermolecular C-H... π interactions with distance of 2.543, 2.633 Å in the single-crystal of mP9PCZ.

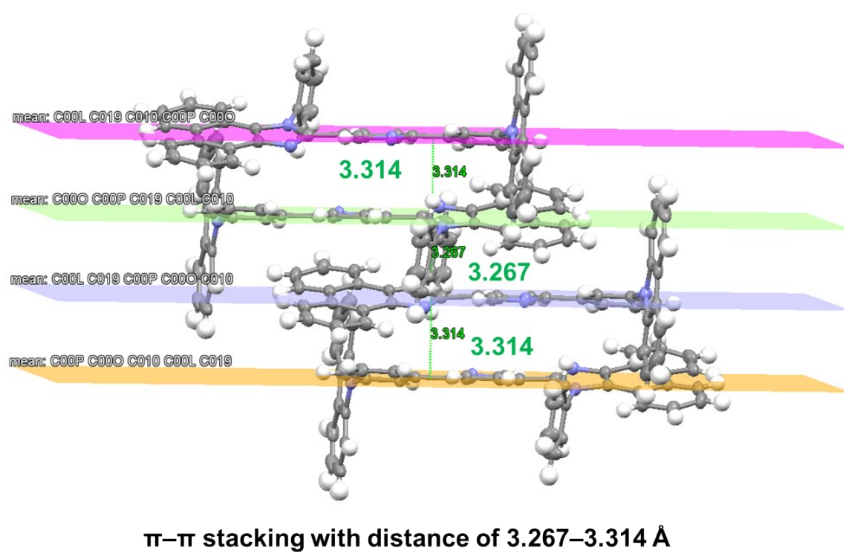
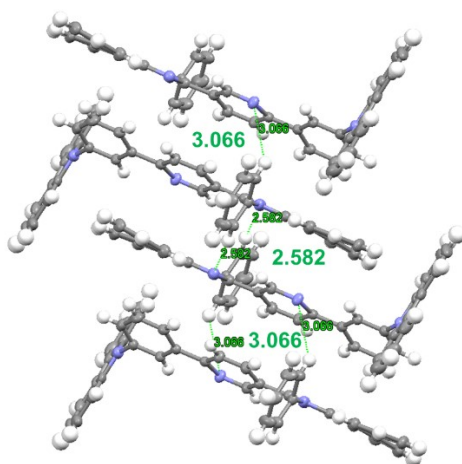
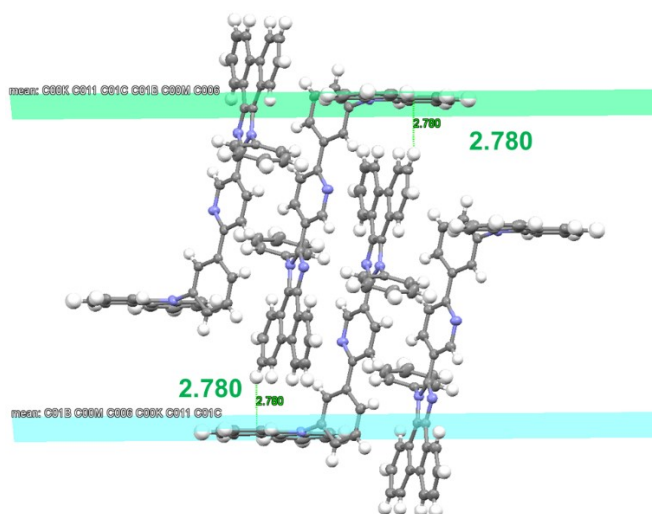


Fig. S4. π - π stacking with distance of 3.267–3.314 Å in the single-crystal of mPmPCZ.



Intermolecular C–H...N interactions: 2.582, 3.066 Å

Fig. S5. Intermolecular C–H...N interactions with distance of 2.582, 3.066 Å in the single-crystal of mPmPCZ.



Intermolecular C–H... π interactions: 2.780 Å

Fig. S6. Intermolecular C–H... π interactions with distance of 2.780 Å in the single-crystal of mPmPCZ.

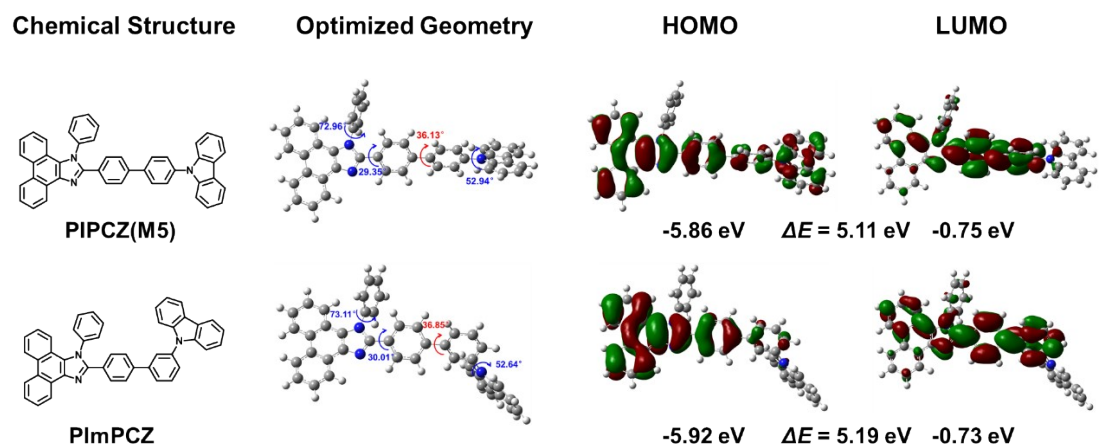


Fig. S7. The molecular structures, calculated optimized structures and HOMO/LUMO distributions of PIPCZ (M5) and PImPCZ.

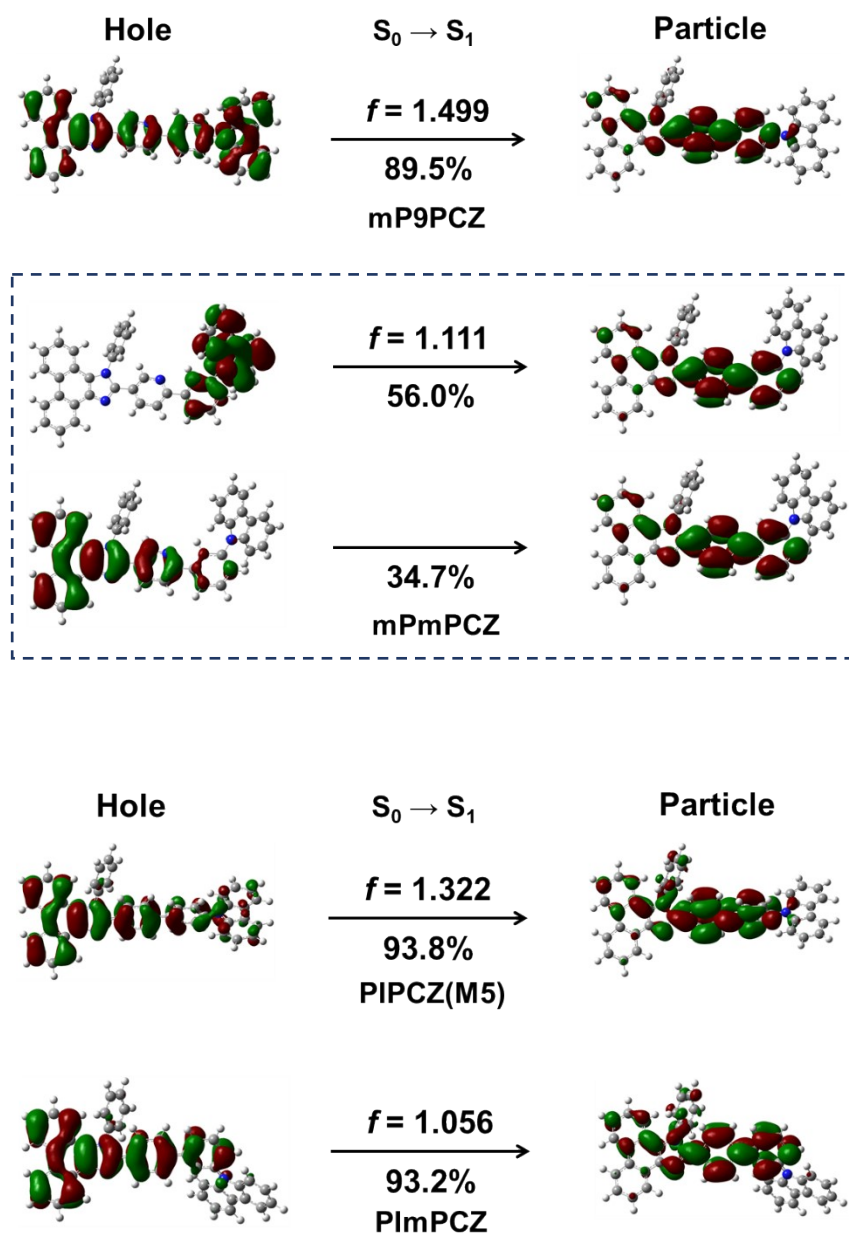


Fig. S8. The natural transition orbitals (NTOs) of $S_0 \rightarrow S_1$ for mP9PCZ, mPmPCZ and their contrastive molecules (PIPCZ and PImPCZ).

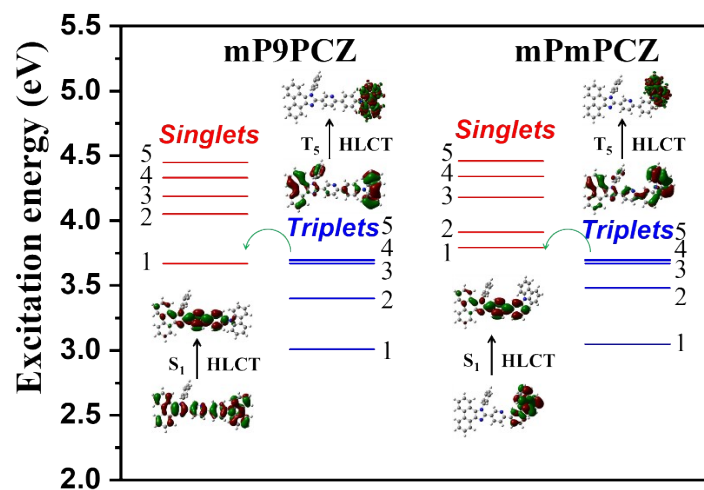


Fig. S9. Energy levels of the first five singlet and triplet excited states in mP9PCZ and mPmPCZ.

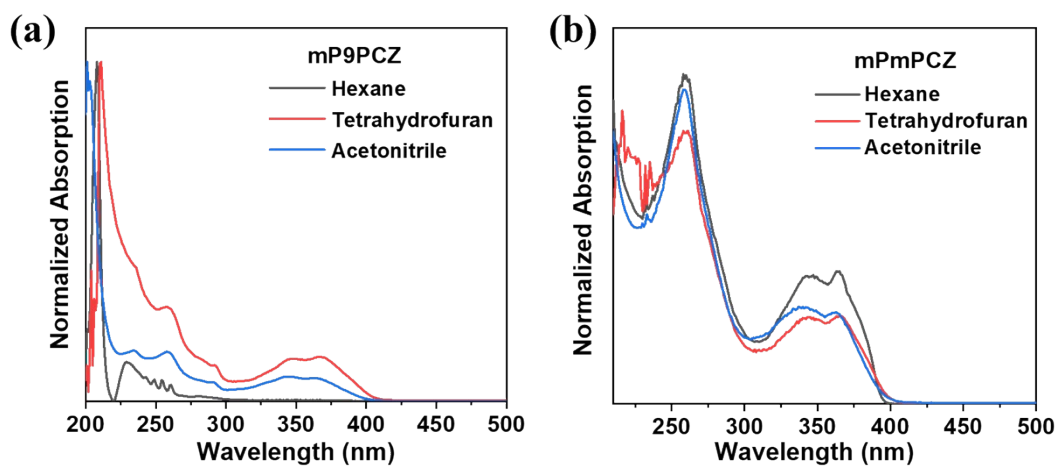


Fig. S10. UV-vis absorption spectra for mP9PCZ (a) and mPmPCZ (b) in different solutions.

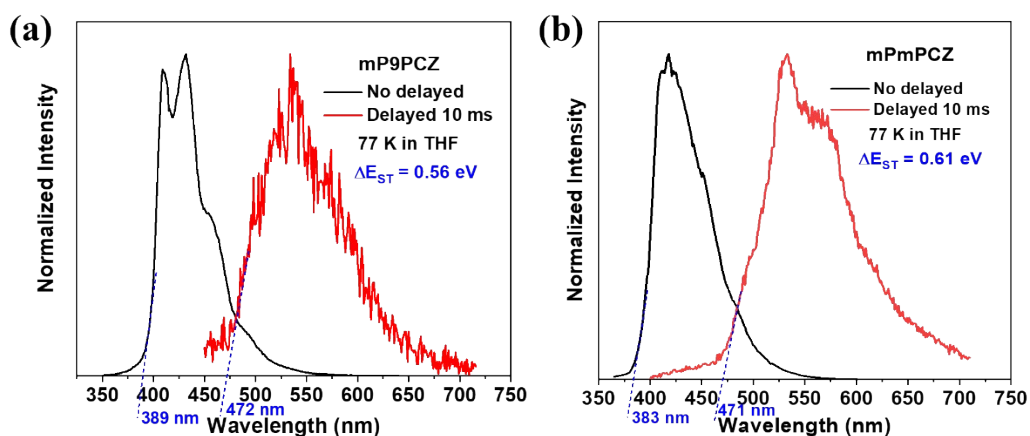


Fig. S11. The fluorescence (Excitation wavelength: 340 nm) and phosphorescence (Excitation wavelength: 390 nm) spectra of mP9PCZ and mPmPCZ in THF at 77 K.

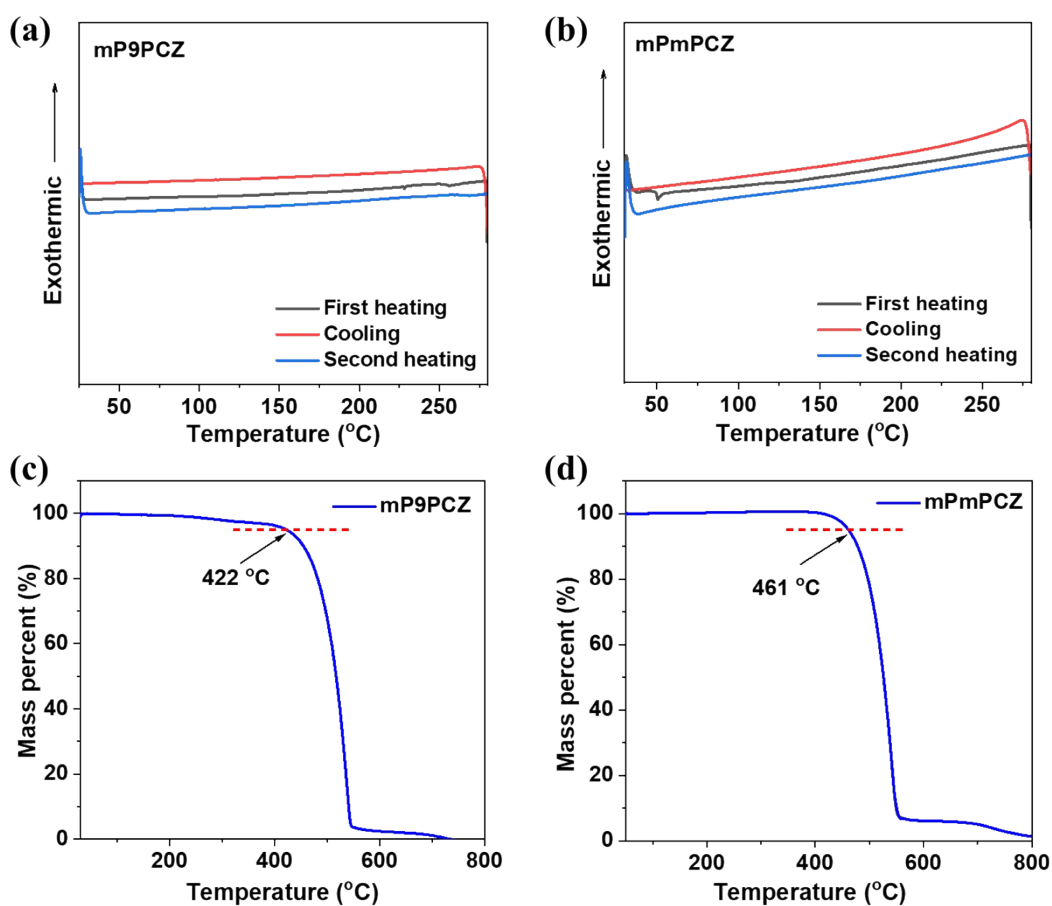


Fig. S12. DSC (a, b) and TGA (c, d) curves of mP9PCZ and mPmPCZ ($10\text{ }^{\circ}\text{C min}^{-1}$ under nitrogen atmosphere).

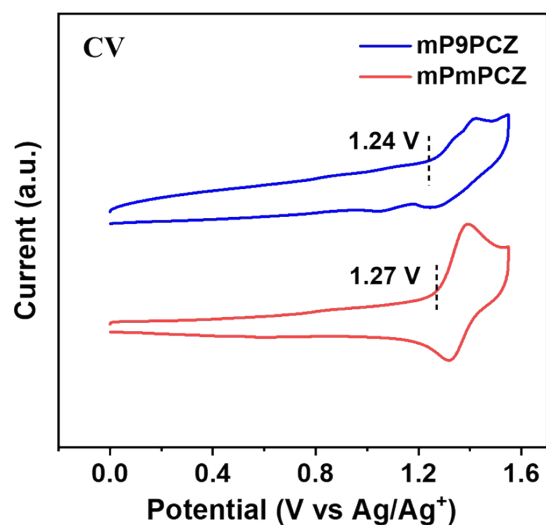


Fig. S13. Cyclic voltammograms of mP9PCZ and mPmPCZ (scan rate: 50 mV s⁻¹).

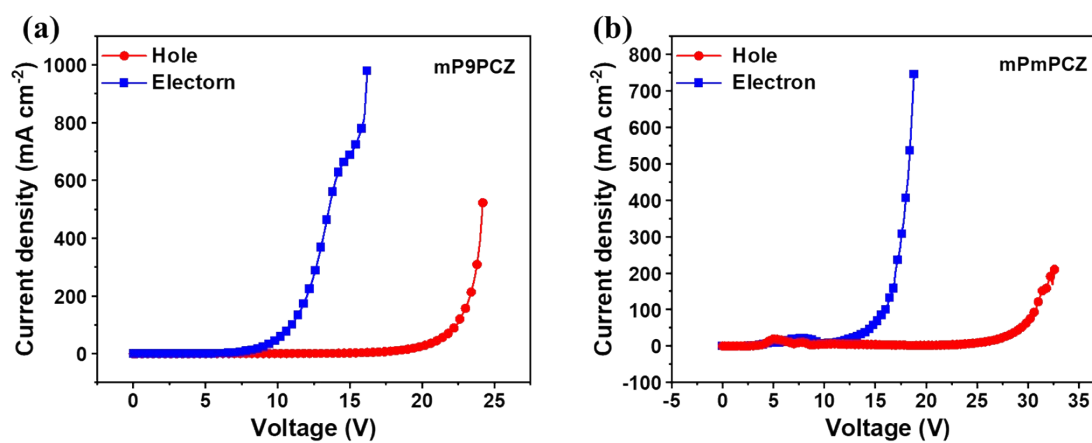


Fig. S14. Plots of current density versus applied voltage of the hole-only and electron-only devices for mP9PCZ and mPmPCZ.

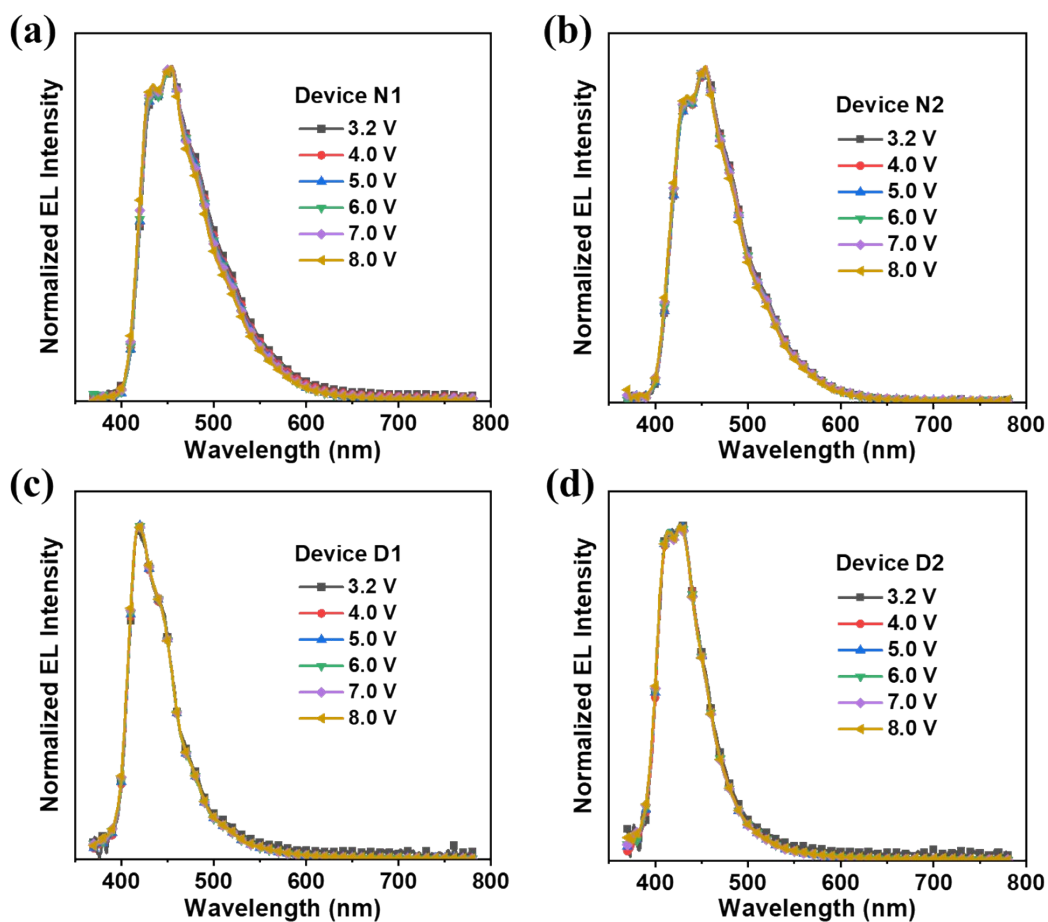


Fig. S15. EL spectra of Device N1 (a) , N2 (b), D1 (c) and D2 (d) under different driving voltages.

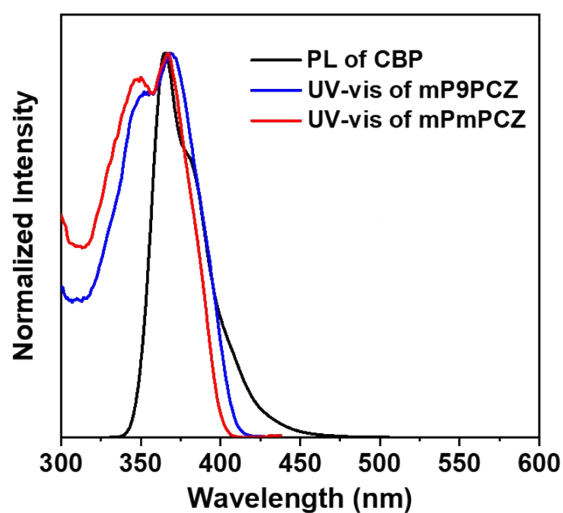


Fig. S16. PL spectrum of CBP and UV-vis absorption spectra of mP9PCZ and mPmPCZ. (Measured in 10^{-5} M toluene solutions.)

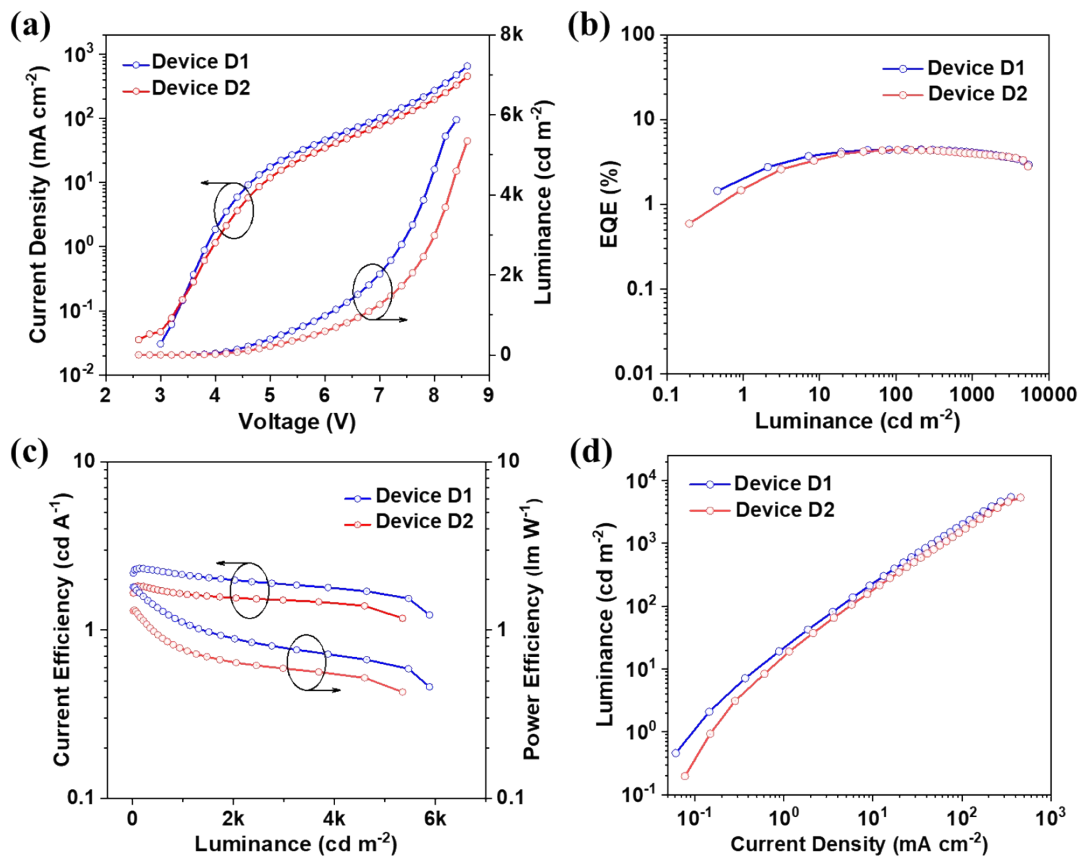


Fig. S17. (a) Current density–voltage–luminance ($J-V-L$), (b) external quantum efficiency–luminance (EQE– L), (c) current efficiency–luminance–power efficiency (CE– L –PE), (d) luminance–current density characteristics of doped devices based on mP9PCZ and mPmPCZ.

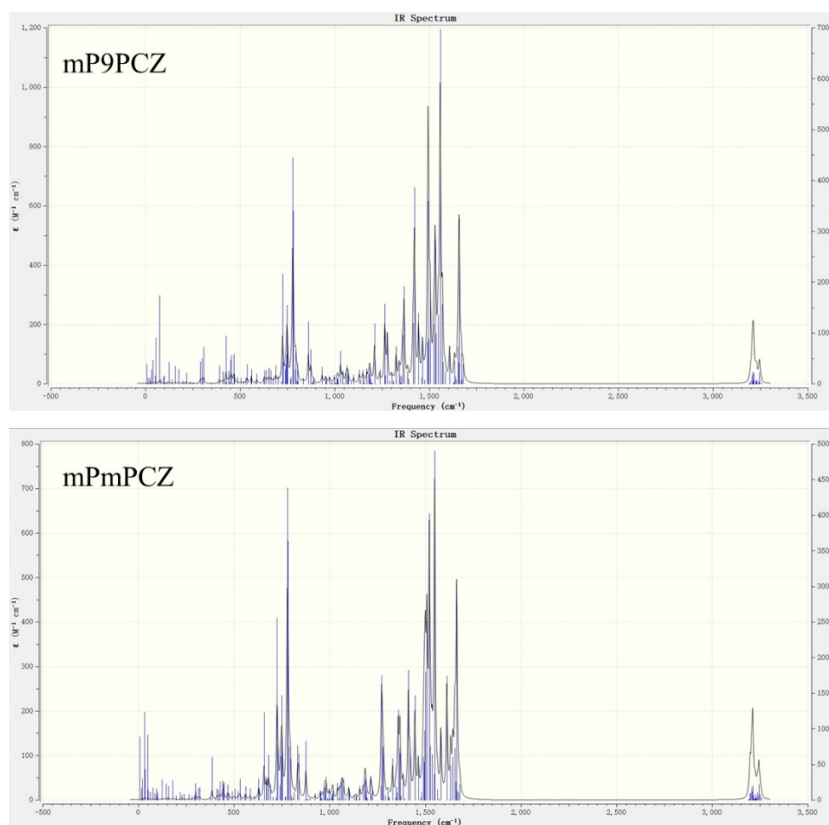


Fig. S18. The vibration frequency analysis of mP9PCZ and mPmPCZ using BMK/6-31g(d,p) basis set.

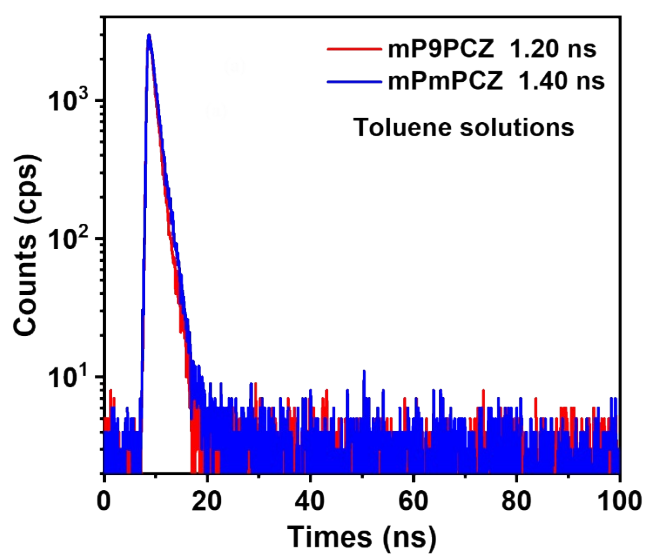


Fig. S19. Transient PL spectra of mP9PCZ and mPmPCZ in toluene solutions.

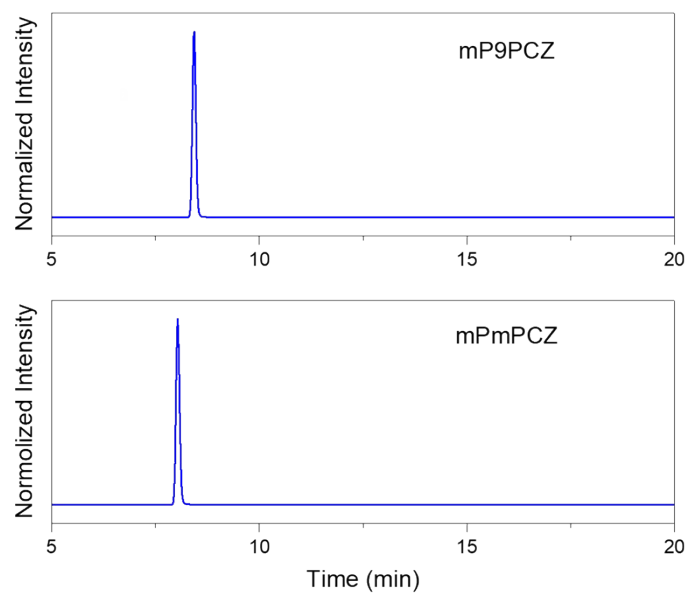
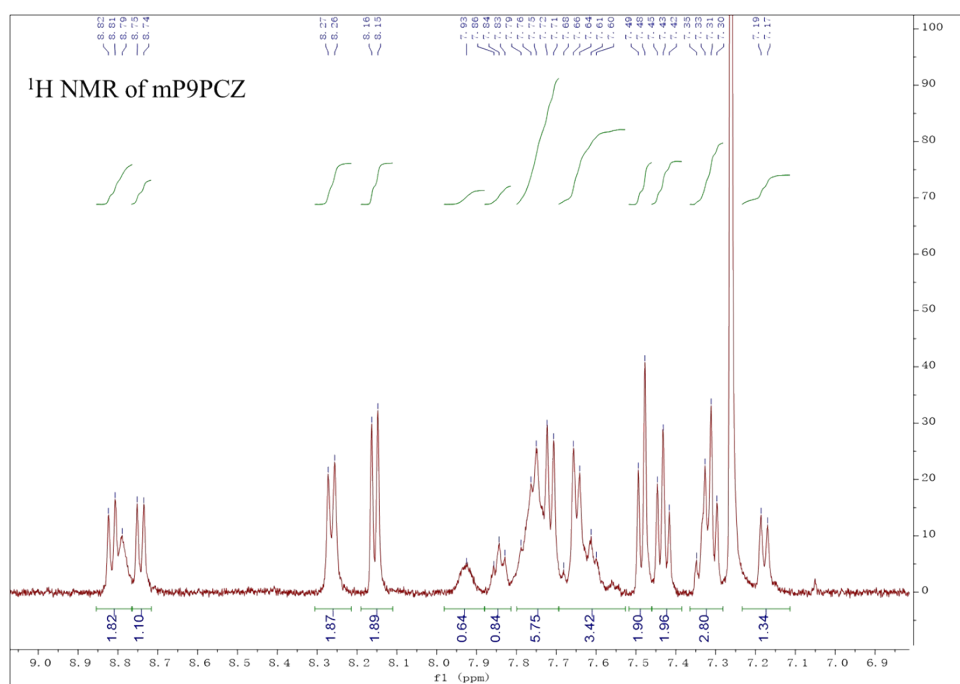


Fig. S20. High-performance liquid chromatography spectra of mP9PCZ and mPmPCZ.



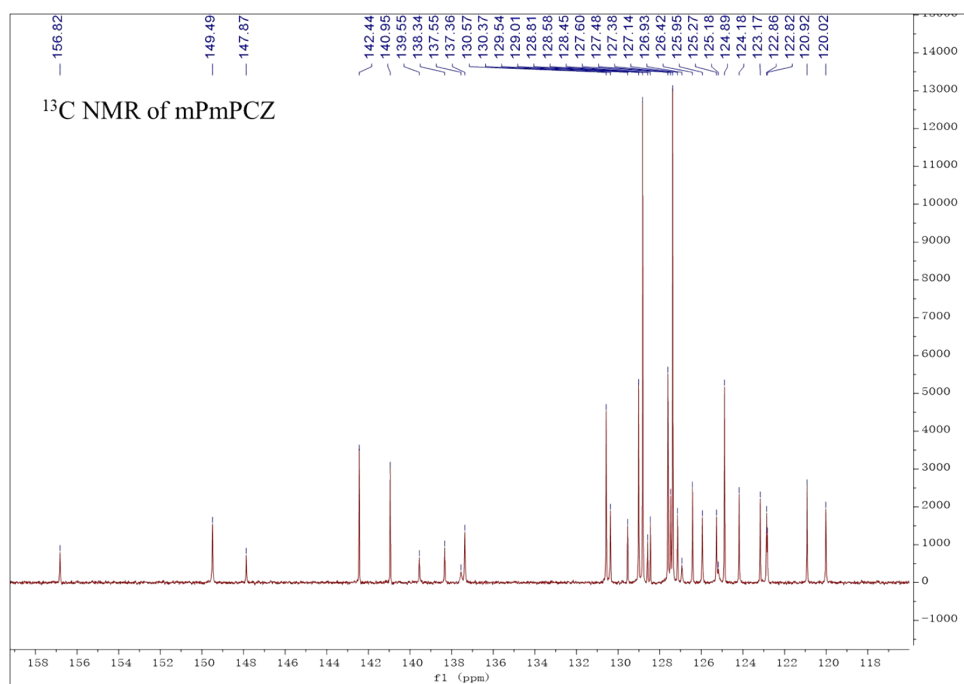


Fig. S22. ¹H and ¹³C NMR of mPmPCZ in CDCl₃.



Fig. S23. Mass Spectrum [M + H]⁺ of mP9PCZ.

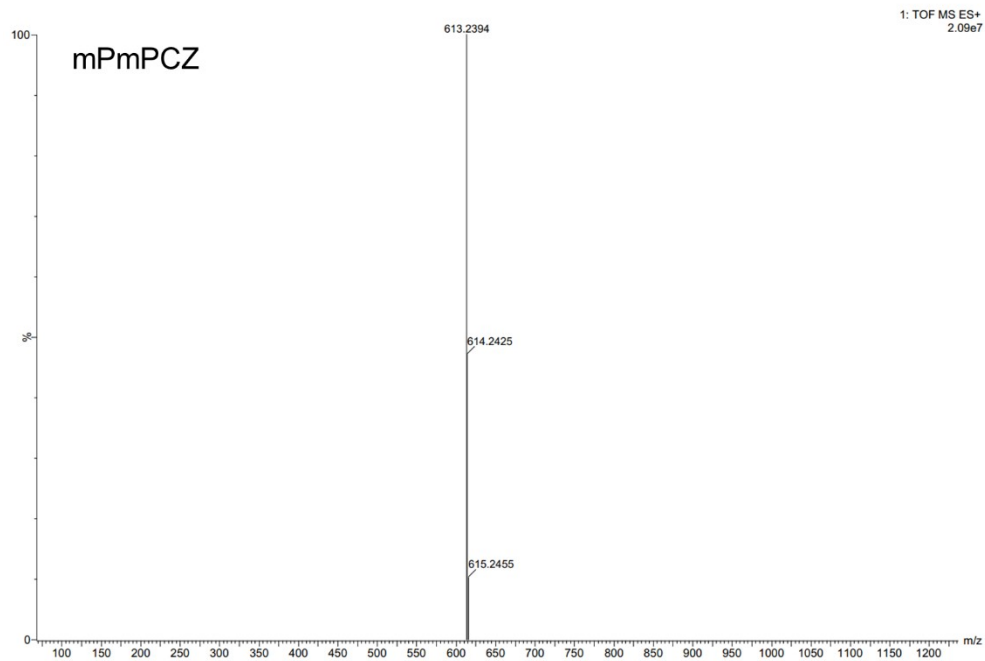


Fig. S24. Mass Spectrum $[M + H]^+$ of mPmPCZ.